A New Coil Structure to Reduce Eddy Current Loss of WPT Systems for Underwater Vehicles

Kehan Zhang, *Member, IEEE*, Xinyi Zhang, Zhengbiao Zhu, Zhengchao Yan, *Student Member, IEEE*, Baowei Song, and Chunting Chris Mi, *Fellow, IEEE*

***Abstract*—Wireless power transfer systems in seawater inevitably suffer some energy loss as a consequence of eddy current loss. Here, we present a coil structure utilizing two transmitter coils placed symmetrically adjacent to each side of the receiver coil. This coil arrangement, termed a $1 \times 1 \times 1$ structure, yields improved power transfer efficiency. The eddy current loss caused by the transmitter coils in a $1 \times 1 \times 1$ system can be reduced to roughly half of that in a 1×1 system, with one transmitter coil and one receiver coil. The experimental results show that the power transfer efficiency from the transmitter to the receiver is improved by nearly 10%. After the introduction of equivalent eddy current loss impedance into the circuit, two arrangements of the $1 \times 1 \times 1$ circuit topology are investigated. They consist of a shared or separately compensated capacitance topology. It is found that the shared-compensated capacitance topology is more robust to the change of mutual inductance than the separately compensated capacitance topology. This kind of structure is very useful in underwater vehicle applications.**

***Index Terms*—Underwater wireless power transfer, two transmitter coils, eddy current loss, robust circuit topology.**

I. Introduction

MANY researchers have studied different approaches in order to achieve higher transfer efficiencies in wireless power transfer (WPT) systems. By utilizing a pair of resonant coils with 10-cm diameter, the series-shunt mixed-resonant circuit was used to achieve a high efficiency of 85% at a relative distance of 10 cm [1]. Besides, the LCC compensation network topology was verified to realize robust reaction in dynamic wireless charging application [2]. Q. Zhu *et al.* focused on the optimization of the compensation capacitors and proposed a novel frequency tuning method based on equivalent circuit model analysis, ultimately achieving a transfer efficiency of 92% over 21-cm distance [3]. Coplanar printed spiral coils and a printed loop were proposed to be applied in manufacturing transmitter and receiver coils. A stable transfer efficiency up to 81.68% was achieved at a distance of 10 cm due to the decreased resistance and the increased quality factor of the printed spiral coil resonators [4]. G. Sakemi *et al.* adopted a method of changing the resonant frequency and derived the trade-off resonant frequency at various transmission distances by numerical simulations to improve the transfer efficiency [5]. The efficiency can be increased by improving the performance of the inverter. G. Scarciotti *et al.* studied the steady-state response of power inverters with non-ideal switches [6]. The Z-source converter was introduced to correct the power factor in WPT applications in [7]. Apart from that the novel near-field capacitively coupled resonators was utilized to get a high efficiency [8]. The combined inductive and capacitive coupling WPT system was proposed, which achieved 2.84-kW output power with 94.5% efficiency at 1 MHz switching frequency [9].

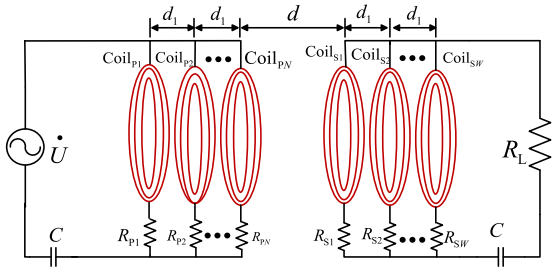

Fig. 1. Schematic of N×W WPT system.

In the field of different coil structures, the three-coil and four-coil structures have better performance on the transmission power and efficiency [10], [11]. Fig. 1 is the schematic of the stacked coils proposed in [12]–[14], which differ from the 1×1 structure and consist of multiple transmitter coils (Coil_{P1}, $\mathrm{Coil}_{P2} \cdots \mathrm{Coil}_{PN}$) connected in parallel with the transmitter side circuit and multiple receiver coils (Coil_{S1}, $\mathrm{Coil}_{S2} \cdots \mathrm{Coil}_{SW}$) connected in parallel to the receiver side circuit ($N \times W$ structure). Sukjin Jim *et al.* investigated the transfer efficiency for three cases: a single coil to a single coil, a single coil to a multi-stacked coil, and a multi-stacked coil to a multi-stacked coil. The simulation results showed that the transfer efficiency of the multi-stacked coil to multi-stacked coil ranked first while that of the single coil to single coil ranked last [12]. Shi Pu and Hon Tat Hui designed a 3×3 structured WPT system with a transfer efficiency of 84% over a mid-range distance of 0.5 m. They also compared the robustness of the 3×3 and 1×1 coil structures over a range of power transfer distances [13]. These results led to the design guidelines proposed by J.P.K. Sampath *et al.*: first,

Manuscript received May 30, 2018; revised September 19, 2018; accepted November 19, 2018. Date of publication November 26, 2018; date of current version January 15, 2019. This work was supported in part by the Natural Science Basic Research Plan in Shaanxi Province of China under Grant 2018JM5033 and in part by the China Scholarship Council under Grant 201806295003. The review of this paper was coordinated by Prof. A. Rathore. *(Corresponding author: Xinyi Zhang.)*

K. Zhang, X. Zhang, Z. Zhu, Z. Yan, and B. Song are with the School of Marine Science and Technology, Northwestern Polytechnical University, Xi'an 710072, China (e-mail: zhangkehan210@163.com; 2624738981@qq.com; we0109@mail.nwpu.edu.cn; yanzc1991@gmail.com; songbaowei@nwpu.edu.cn).

C. C. Mi is with theDepartment of Electrical and Computer Engineering, San Diego State University, San Diego, CA 92182, USA (e-mail: mi@ieee.org).

Color versions of one or more of the figures in this paper are available online at http://ieeexplore.ieee.org.

Digital Object Identifier 10.1109/TVT.2018.2883473

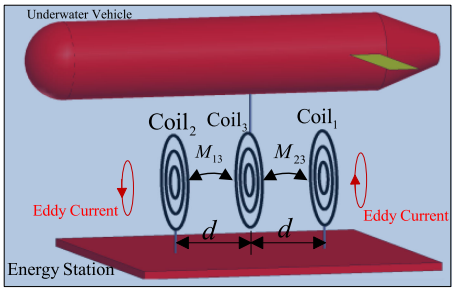

Fig. 2. Wireless power transfer in seawater with 1 × 1 × 1 structure.

choose a substantial value of separation between turns to reduce proximity effect losses; second, maximize possible number of turns within the footprint area; finally, optimize the number of layers in the coil structure with selective design parameters [14].

WPT technology is mainly applied in open air, such as in electric vehicles, medical applications, cellphones and so on [15]. However, the future of undersea WPT is also bright. The traditional way of recharging autonomous underwater vehicles (AUVs) is time-consuming, while the WPT technology is regarded as a potential solution to recharge them more quickly [16]. Once an AUV runs out of power, it docks at an energy station, as shown in Fig. 2. While the energy station supplies power to the AUV, data gathered by the AUV are transferred to the energy station. The exchange of power and data is accomplished without manual intervention, which is safe and convenient.

One of the most remarkable differences between WPT systems in seawater and air is that the electric field passing through the seawater causes the eddy current loss. The eddy current loss inevitably impairs the transfer efficiency of the systems [17], [18]. Additionally, coils are usually placed in a box with a thick board against high pressure seawater, increasing the distance from the transmitter to the receiver. The distance may be 100 mm or even longer. The coil diameter is also restricted by the shape and volume of the AUV, usually ranging from 50 to 150 mm. As a result, the mutual inductance is small. For example, the largest mutual inductance in our experiment is 5.6 μH, with a load resistance of 31.5 Ω. Therefore, the reflected resistance is less than 2 Ω, while the resonant frequency is 200 kHz. One way to improve the reflected resistance is to increase the frequency. However, the increase of frequency leads to the higher eddy current loss in seawater WPT systems. Therefore, in these systems, it is vital to reduce eddy current loss at high frequency to improve their transfer efficiencies.

In this paper, we take the simple case of two transmitter coils, Coil_1 and Coil_2, which are connected in parallel with the energy station and arranged symmetrically adjacently to a single receiver coil, Coil_3. This arrangement is adopted to improve the transfer efficiency and herein is referred to as a 1 × 1 × 1 structure, as shown in Fig. 2. Section II discusses that a 1 × 1 × 1 structure can reduce the eddy current loss generated by the two transmitter coils compared with 1 × 1 structure with one transmitter coil and one receiver coil. Introducing the equivalent eddy current loss impedance into the circuit, Section III analyzes the circuit model of a 1 × 1 × 1 structure. Section IV describes a shared-compensated capacitance topology to improve the stability of the 1 × 1 × 1 structure with regard to the change of mutual inductance either between Coil_1 and Coil_3 or between Coil_2 and Coil_3. Section V demonstrates the experimental platform and presents the results of the study.

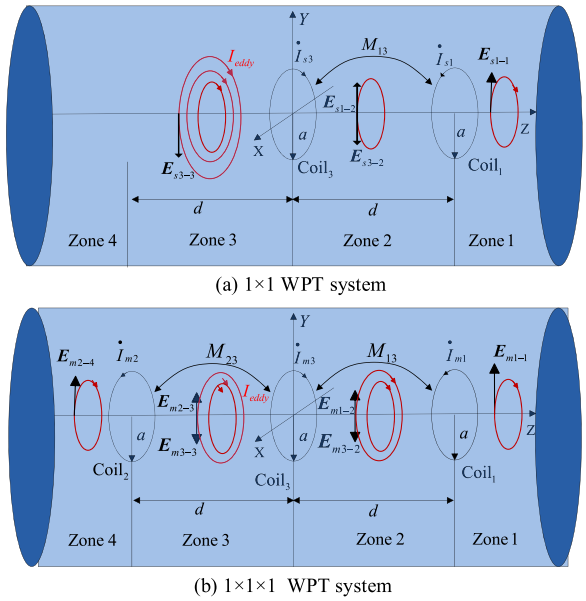

Fig. 3. Electric field distribution in seawater.

II. Eddy Current Loss Analysis of Underwater WPT Systems

In this section, the electric fields of a 1 × 1 system, as depicted in Fig. 3(a), and a 1 × 1 × 1 system, as depicted in Fig. 3(b), are analyzed, and the eddy current losses in the two systems are compared. In Fig. 3(a), the center coordinates of the transmitter coil, Coil_1, and the receiver coil, Coil_3, are (0, 0, d) and (0, 0, 0), respectively. In the 1 × 1 × 1 configuration, there is another transmitter coil, Coil_2, shown in Fig. 3(b), centered at $(0, 0, -d)$. In Fig. 3(a), M_{13} is the mutual inductances between Coil_1 and Coil_3. $\boldsymbol{I}_{\mathrm{s}1}$ and $\boldsymbol{I}_{\mathrm{s}3}$ represent the current of the Coil_1 and Coil_3 respectively. $\boldsymbol{E}_{\mathrm{s}i-j}$ represents the electric field excited by Coil_i in Zone j. In Fig. 3(b), M_{13} and M_{23} are the mutual inductances between Coil_1 and Coil_3 and between Coil_2 and Coil_3, respectively. $\boldsymbol{I}_{\mathrm{m}1}$, $\boldsymbol{I}_{\mathrm{m}2}$ and $\boldsymbol{I}_{\mathrm{m}3}$ represent the current of the Coil_1, Coil_2 and Coil_3 respectively. $\boldsymbol{E}_{\mathrm{m}i-j}$ represents the electric field excited by Coil_i in Zone j.

The coil parameters examined in this paper are as follows: the inner radius is 50 mm, the outer radius is 110 mm, the number of coil turns is 15.

The major eddy current loss zone is divided into four subzones:

$$\begin{aligned}
&\mathrm{Zone\,4}: x_{\min} \le x \le x_{\max}, y_{\min} \le \mathrm{y} \le y_{\max}, z_{\min} \le z \le -d;\\
&\mathrm{Zone\,3}: x_{\min} \le x \le x_{\max}, y_{\min} \le \mathrm{y} \le y_{\max}, -d < z \le 0;\\
&\mathrm{Zone\,2}: x_{\min} \le x \le x_{\max}, y_{\min} \le \mathrm{y} \le y_{\max}, 0 < z \le d;\\
&\mathrm{Zone\,1}: x_{\min} \le x \le x_{\max}, y_{\min} \le \mathrm{y} \le y_{\max}, d < z \le z_{\max}.
\end{aligned}$$

To precisely calculate the total eddy current loss, the eddy current loss zone must be large enough to account for all relevant effects in the finite element simulation. Otherwise, the calculation results will be smaller than the experiment results.

Finite element analysis software is used to calculate the electric field intensity of the WPT systems. In the 1 × 1 system, the electric field intensities in the *YOZ* plane are given in Fig. 4(a)

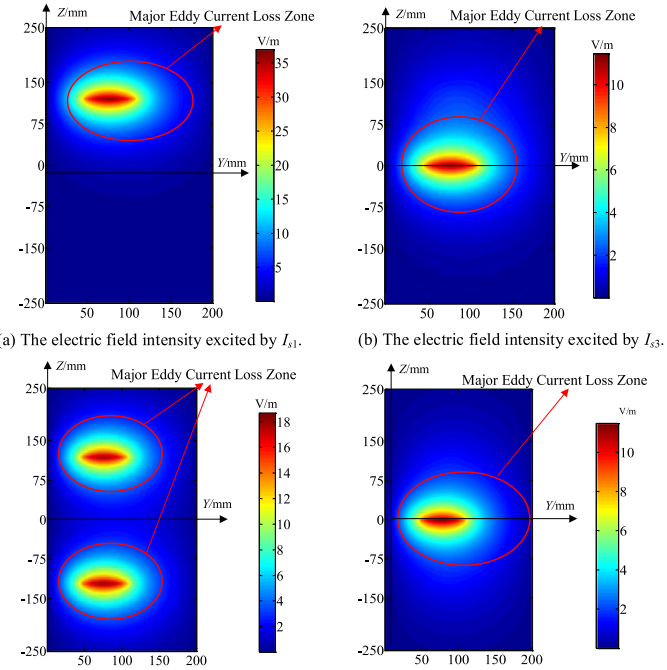

(a) The electric field intensity excited by I_{s1}. (b) The electric field intensity excited by I_{s3}.

(c)The electric field intensity excited by I_{m1} and I_{m2}. (d)The electric field intensity excited by I_{m3}.

Fig. 4. The electric field distribution of different coil structures ($I_{s1} = 1.7$ A, $R_L = 30\ \Omega$, $I_{s3} = I_{m3} = 0.5$ A, $f = 600$ kHz, $I_{m1} = I_{m2} = 0.85$ A, and $\sigma = 4$ S/m. The simulation parameters in Fig. 5 is the same as those in Fig. 4).

and (b). In the $1 \times 1 \times 1$ system, the electric field intensities are given in Fig. 4(c) and (d). Because these coils have *Z*-axial symmetry, the electric field intensity in *YOZ* plane also has *Z*-axial symmetry and the electric field distribution in any other planes crossing the *Z*-axis are the same as that in *YOZ* plane. The root mean square current, I_{s1}, in the transmitter coil of the 1×1 system is 1.7A. I_{m1} and I_{m2} are both 0.85 A. Comparing Fig. 4(a) and (c), it is evident that the electric field intensity excited by transmitter coils in the $1 \times 1 \times 1$ system is only half of that excited by transmitter coil in 1×1 system, but the major eddy current loss zone is twice as large. By comparing Fig. 4(b) and (d), it is evident that the electric field intensities excited by the receiver coils in both the 1×1 system and the $1 \times 1 \times 1$ system are the same, which indicates that the power transferred to the receiver side is the same and the eddy current loss caused by the receiver coils is also the same.

The module of electric field intensities is given in Fig. 5. By comparing Fig. 4(c), (d) and Fig. 5(b), it can be observed that the electric field intensity is only determined by the current I_{m1} in Zone 1. At the same time, the electric field intensity in Zone 2 is determined by both I_{m1} and I_{m3}. The electric field close to the transmitter coils in Zone 2, and Zone 3 is mainly determined by the current in the transmitter coils, while the current in the receiver coil has little influence on it. Similarly, the electric field intensity at coordinates close to the receiver coil is mainly determined by current in the receiver coil. In the overlap zones marked in Fig. 5(b), the electric field intensity is the synthesis of $\boldsymbol{E}_{m1-2}$ and $\boldsymbol{E}_{m3-2}$ (or $\boldsymbol{E}_{m2-3}$ and $\boldsymbol{E}_{m3-3}$).

Because the overlap zone is small, as shown in Fig. 5, the phase difference between $\boldsymbol{E}_{m1-2}$ and $\boldsymbol{E}_{m3-2}$ (or $\boldsymbol{E}_{m2-3}$ and $\boldsymbol{E}_{m3-3}$) is treated as 90 degrees to simplify the calculations for eddy current loss in the following equations (1) to (6) [19].

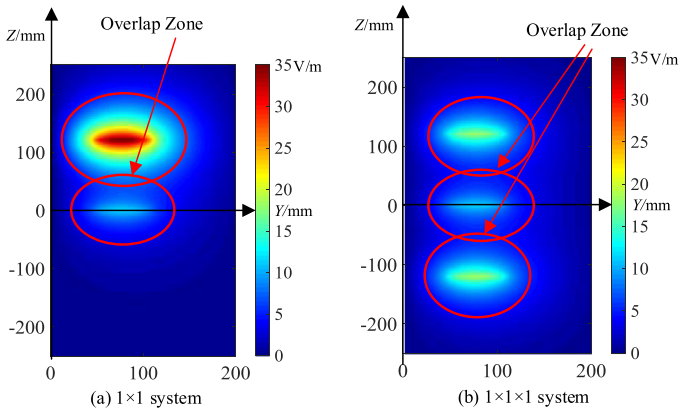

(a) 1×1 system (b) 1×1×1 system

Fig. 5. The modulus of electric field intensity.

The synthetic electric field in Zone 2 of the $1 \times 1 \times 1$ system can be expressed as follows:

$$\begin{aligned}\boldsymbol{E}_{\text{total}}(x,y,z) &= \boldsymbol{E}_{\text{m3-2}}(x,y,z) + \boldsymbol{E}_{\text{m1-2}}(x,y,z)\\ &\approx \sqrt{2}E_{\text{m3-2}}(x,y,z)sin(\omega t)\\ &\quad + \sqrt{2}E_{\text{m1-2}}(x,y,z)sin\left(\omega t + \frac{\pi}{2}\right)\\ &= \sqrt{2}\sqrt{E^2_{\text{m3-2}}(x,y,z) + E^2_{\text{m1-2}}(x,y,z)}\\ &\quad \times \sin(\omega t + \phi)\\ &= \sqrt{2}E_{\text{total}}(x,y,z)\sin(\omega t + \phi) \qquad (1)\end{aligned}$$

In the overlap zone of Zone 2, the following equation is used to calculate eddy current loss:

$$E_{\text{total}}(x,y,z) = \sqrt{E^2_{\text{m3-2}}(x,y,z) + E^2_{\text{m1-2}}(x,y,z)}$$

The eddy current loss of $1 \times 1 \times 1$ system in Zone 2 is:

$$\begin{aligned}P_{\text{Zone2}} &= \sigma \iiint E^2_{\text{total}}(x,y,z)dV_2\\ &= \sigma \iiint (E^2_{\text{m3-2}}(x,y,z) + E^2_{\text{m1-2}}(x,y,z))dV_2 \qquad (2)\end{aligned}$$

And then the total eddy current loss of $1 \times 1 \times 1$ system is:

$$\begin{aligned}P_{\text{eddy\_m}} = \sigma \Bigg[&\iiint E^2_{m1-1}(x,y,z)dV_1 + \iiint (E^2_{m1-2}(x,y,z)\\ &+ E^2_{m3-2}(x,y,z))dV_2\\ &+ \iiint (E^2_{m3-3}(x,y,z) + E^2_{m2-3}(x,y,z))dV_3\\ &+ \iiint E^2_{m2-4}(x,y,z)dV_4 \Bigg] \qquad (3)\end{aligned}$$

Similarly, the total eddy current loss of 1×1 system is:

$$P_{\text{eddy\_s}} = \sigma \Bigg[\iiint E_{s1-1}^2(x,y,z)dV_1 + \iiint (E_{s1-2}^2(x,y,z) + E_{s3-2}^2(x,y,z))dV_2 + \iiint E_{s3-3}^2(x,y,z)dV_3 \Bigg] \tag{4}$$

where V_1, V_2, V_3, and V_4 are the integral volumes in Zone 1, 2, 3, 4, respectively.

To compare the eddy current losses of the 1×1 and the $1 \times 1 \times 1$ systems when the power transferred to the receiver side of each system is equal, I_{m3} is set to be equivalent to I_{s3}, the following expressions is obtained [19]:

$$I_{\text{m1}} = I_{\text{m2}} = \frac{1}{2} I_{\text{s1}} \tag{5}$$

$$\begin{aligned} P_{\text{eddy\_reduced}} &= P_{\text{eddy\_s}} - P_{\text{eddy\_m}} \\ &= \frac{1}{2}\sigma \Bigg[\iiint E_{s1-1}^2(x,y,z)dV_1 + \iiint E_{s1-2}^2(x,y,z)dV_2 \Bigg] \end{aligned} \tag{6}$$

Equation (6) shows that the reduction of the eddy current loss in the $1 \times 1 \times 1$ system is equal to half of the eddy current loss of the transmitting coil in the 1×1 system.

III. The Circuit Model of the Underwater WPT System

As a designer, we care more about the influence of the circuit parameters on changing the transfer efficiency of the system and ultimately the transferred power to the load. Therefore, it is necessary to find an equivalent circuit model of the $1 \times 1 \times 1$ WPT system.

Since $E_{\text{m}i-j}$ is proportional to $I_{\text{m}i}$, the total eddy current loss in (3) can be expressed as follows:

$$P_{\text{eddy\_m}} = R_{\text{eddy1}} I_{\text{m1}}^2 + R_{\text{eddy2}} I_{\text{m2}}^2 + R_{\text{eddy3}} I_{\text{m3}}^2 \tag{7}$$

where R_{eddy1}, R_{eddy2}, and R_{eddy3} are the equivalent eddy current loss impedance (EECLI). EECLI can be obtained through the following equations:

$$\begin{cases} \sigma[\iiint E_{m1-1}^2(x,y,z)dV_1 + \iiint E_{m1-2}^2(x,y,z)dV_2] = R_{\text{eddy1}} I_{\text{m1}}^2 \\ \sigma[\iiint E_{m2-3}^2(x,y,z))dV_3 + \iiint E_{m2-4}^2(x,y,z)dV_4] = R_{\text{eddy2}} I_{\text{m2}}^2 \\ \sigma[\iiint E_{m3-2}^2(x,y,z)dV_2 + \iiint E_{m3-3}^2(x,y,z)dV_3] = R_{\text{eddy3}} I_{\text{m3}}^2 \end{cases} \tag{8}$$

According to (8), it can be known that the influence of eddy current loss on WPT systems can be represented by a resistance. Therefore, the equivalent circuit model of an underwater WPT system can be expressed as shown in Fig. 6, where R_{Coil1}, R_{Coil2} and R_{Coil3} are the coil impedances. The introduction of EECLI greatly simplifies the analysis of the transfer efficiency under different mutual inductances.

Fig. 6 depicts the circuit topology that is referred to as the separately compensated topology of the $1 \times 1 \times 1$ system in seawater. C_1 and C_2 are respectively added to Branch 1 and Branch 2 to ensure that $\dot{I}_{\text{m1}}$, $\dot{I}_{\text{m2}}$ and $\dot{U}$ are in phase at the angular frequency, ω. Compared with M_{13} and M_{23}, M_{12} is tiny and does not have a significant influence on the system. R_1, R_2 and R_3 are the sum of the coil impedance and the EECLI. R_{L} is the load resistance. The RMS value of the inductive voltage in Coil_3 excited by $\dot{I}_{\text{m1}}$ and $\dot{I}_{\text{m2}}$ is expressed as:

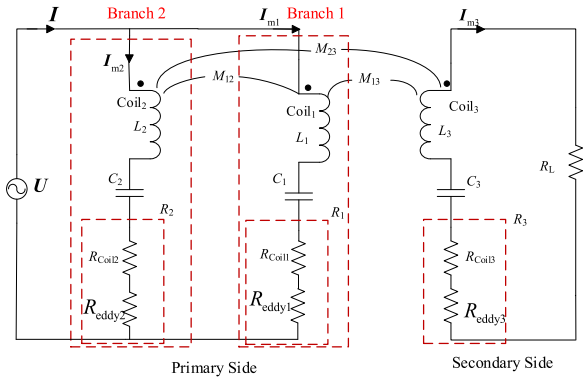

Fig. 6. The separately compensated capacitance topology.

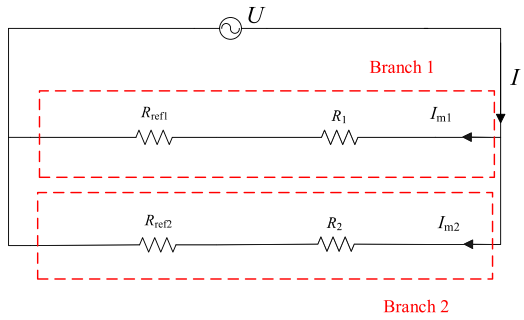

Fig. 7. The equivalent circuit of primary side.

$$U_3 = \omega M_{13} I_{\text{m1}} + \omega M_{23} I_{\text{m2}} \tag{9}$$

The resonance current in the receiver, I_{m3} is expressed as:

$$I_{\text{m3}} = \frac{U_3}{R_{\text{L1}}} = \frac{\omega(M_{13} I_{\text{m1}} + M_{23} I_{\text{m2}})}{R_{\text{L}} + R_3} \tag{10}$$

The power transferred to the receiver coil is:

$$\begin{aligned} P_L &= \frac{U_3^2}{R_{\text{L1}}} = \frac{(\omega M_{13} I_{\text{m1}} + \omega M_{23} I_{\text{m2}})^2}{R_{\text{L}} + R_3} \\ &= \omega M_{13} I_{\text{m1}} I_{\text{m3}} + \omega M_{23} I_{\text{m2}} I_{\text{m3}} \end{aligned} \tag{11}$$

The power $\omega M_{13} I_{\text{m1}} I_{\text{m3}}$ is provided by Coil_1, and $\omega M_{23} I_{\text{m2}} I_{\text{m3}}$ is provided by Coil_2. Therefore, the equivalent reflected resistances in each branch are:

$$R_{\text{ref1}} = \frac{\omega M_{13} I_{\text{m1}} I_{\text{m3}}}{I_{\text{m1}}^2} = \frac{\omega^2 M_{13}(M_{13} I_{\text{m1}} + M_{23} I_{\text{m2}})}{I_{\text{m1}} R_{\text{L1}}} \tag{12}$$

$$R_{\text{ref2}} = \frac{\omega M_{23} I_{\text{m2}} I_{\text{m3}}}{I_{\text{m2}}^2} = \frac{\omega^2 M_{23}(M_{13} I_{\text{m1}} + M_{23} I_{\text{m2}})}{I_{\text{m2}} R_{\text{L1}}} \tag{13}$$

Fig. 7 is the primary circuit model, while both Branch 1 and Branch 2 are in the resonance state. According to Kirchhoff's law, the RMS value of the power source voltage can be

expressed as:

$$U = (R_{\mathrm{ref1}} + R_1) I_{\mathrm{m1}} = \frac{\omega^2 M_{13}(M_{13} I_{\mathrm{m1}} + M_{23} I_{\mathrm{m2}})}{R_{\mathrm{L1}}} + R_1 I_{\mathrm{m1}} \tag{14}$$

$$U = (R_{\mathrm{ref2}} + R_2) I_{\mathrm{m2}} = \frac{\omega^2 M_{23}(M_{13} I_{\mathrm{m1}} + M_{23} I_{\mathrm{m2}})}{R_{\mathrm{L1}}} + R_2 I_{\mathrm{m2}} \tag{15}$$

Let:

$$\begin{cases} R_{\mathrm{ref}} = \frac{(\omega M_{13})^2}{R_{\mathrm{L1}}} \\ \alpha = \frac{M_{13}}{M_{23}} \\ k = \frac{I_{\mathrm{m2}}}{I_{\mathrm{m1}}} \end{cases}$$

Then, the total resistances in Branch 1 and Branch 2 are expressed as:

$$\begin{cases} R_{1\_\mathrm{real}} = R_{\mathrm{ref}} + \frac{R_{\mathrm{ref}} k}{\alpha} + R_1 \\ R_{2\_\mathrm{real}} = \frac{R_{\mathrm{ref}}}{\alpha^2} + \frac{R_{\mathrm{ref}}}{\alpha k} + R_2 \end{cases} \tag{16}$$

By substituting (16) into the following expression:

$$k = \frac{I_{\mathrm{m2}}}{I_{\mathrm{m1}}} = \frac{U/R_{2\_\mathrm{real}}}{U/R_{1\_\mathrm{real}}} = \frac{R_{1\_\mathrm{real}}}{R_{2\_\mathrm{real}}} \tag{17}$$

k is obtained:

$$k = \frac{\alpha^2 R_1 + R_{\mathrm{ref}} \alpha(\alpha - 1)}{R_{\mathrm{ref}}(1-\alpha) + \alpha^2 R_2} \tag{18}$$

From (18), it can be seen that k is constant as long as the system parameters such as M_{12}, M_{23}, R_1 and R_2 are fixed. Once k is obtained, the transfer efficiency from the primary side to the secondary side $\eta_{\mathrm{P-S}}$ and the total resistance can be obtained:

$$\eta_{\mathrm{P\_S}} = \frac{(R_{\mathrm{ref}} + \frac{R_{\mathrm{ref}} k}{\alpha}) R_{2\_\mathrm{real}}^2 + (\frac{R_{\mathrm{ref}}}{\alpha^2} + \frac{R_{\mathrm{ref}}}{\alpha k}) R_{1\_\mathrm{real}}^2}{R_{1\_\mathrm{real}} R_{2\_\mathrm{real}} (R_{1\_\mathrm{real}} + R_{2\_\mathrm{real}})} \tag{19}$$

$$R_{\mathrm{eql}} = \frac{R_{1\_\mathrm{real}} R_{2\_\mathrm{real}}}{R_{1\_\mathrm{real}} + R_{2\_\mathrm{real}}} \tag{20}$$

The change of $\eta_{\mathrm{P\_S}}$ at different values of M_{23} is given in Fig. 8(a). The mutual inductance M_{13} is constant at 5.56 μH, and the resonance frequency is 600 kHz. From these figures, it is evident that $\eta_{\mathrm{P-S}}$ is falling with the decrease of M_{23}. When M_{23} is larger than the critical points, marked by pentagons, $\eta_{\mathrm{P-S}}$ of the $1 \times 1 \times 1$ system is larger than that of the 1×1 system.

From Fig. 8(b), the ratio of the currents $I_{\mathrm{m2}}/I_{\mathrm{m1}}$ is also changing with M_{23}. When M_{23} is less than 5.56 μH, the ratio $I_{\mathrm{m2}}/I_{\mathrm{m1}}$ is larger than 1. Branch 1 and Branch 2 are both excited by the voltage U. Therefore, the power consumed in Branch 2 is larger than that in Branch 1. In terms of transfer efficiency, according to (13), the decrease of M_{23} results in the decrease of R_{ref2}. Therefore, the transfer efficiency of Branch 2 is smaller than Branch 1. In summary, the decrease of M_{23} brings two disadvantages to the $1 \times 1 \times 1$ system: decreasing the transfer efficiency of Branch 2 and the increasing the injected power into Branch 2. The later effect aggravates the drop in the total transfer efficiency in (19).

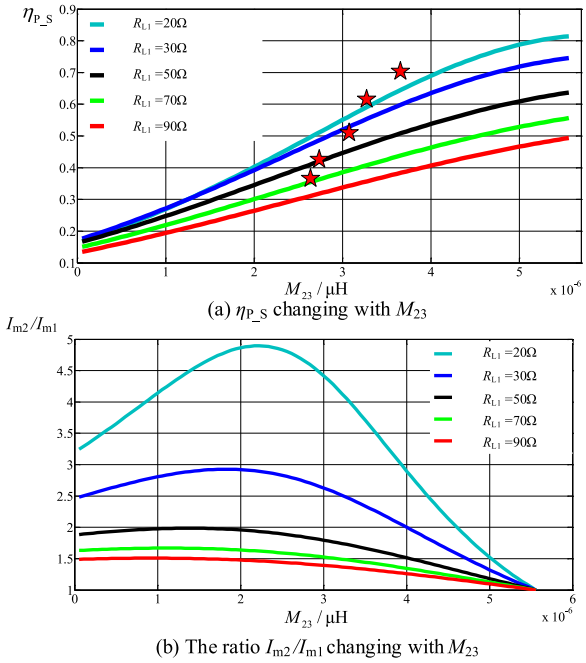

(a) $\eta_{\mathrm{P\_S}}$ changing with M_{23}

(b) The ratio $I_{\mathrm{m2}}/I_{\mathrm{m1}}$ changing with M_{23}

Fig. 8. $\eta_{\mathrm{P\_S}}$ and $I_{\mathrm{m2}}/I_{\mathrm{m1}}$ changing with M_{23} while R_{L1} are 20, 30, 50, 70, 90 Ω. R_1 and R_2 are constant 3 Ω.

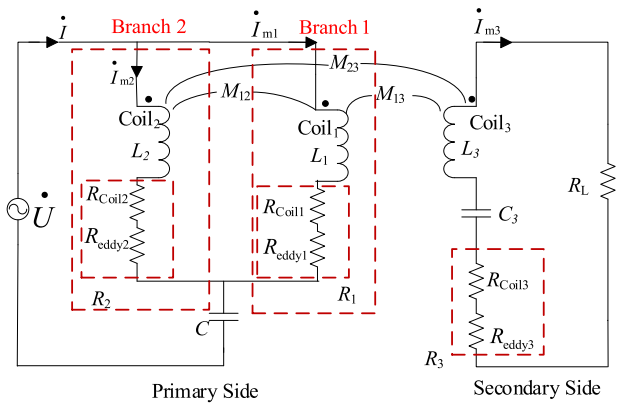

Fig. 9. The shared-compensated capacitance topology.

IV. The Shared-Compensated Capacitance Topology

In some cases, the coil gap between Coil$_2$ and Coil$_3$ may be larger than that between Coil$_1$ and Coil$_3$, or the relative position of underwater vehicle to the energy station is disturbed by unexpected factors, resulting in a change to M_{23}. To enhance the robustness of the $1 \times 1 \times 1$ structure versus mutual inductance change, the shared-compensated capacitance topology in Fig. 9 is proposed.

In Branch 1, the impedance ωL_1 is usually tens of or even hundreds of ohms. But in seawater systems, the coupling coefficient of the transmitter and receiver coils is usually 0.1 or less. As a result, the equivalent reflected resistance R_{ref1} is much smaller than ωL_1. Because of that, the current I_{m1} is mainly determined by ωL_1 in the shared-compensated capacitance topology. The situation is the same in Branch 2.

When ωL_1 and ωL_2 are equivalent, the ratio of I_{m1} to I_{m2} is close to 1. Therefore, the transfer efficiency from the transmitter

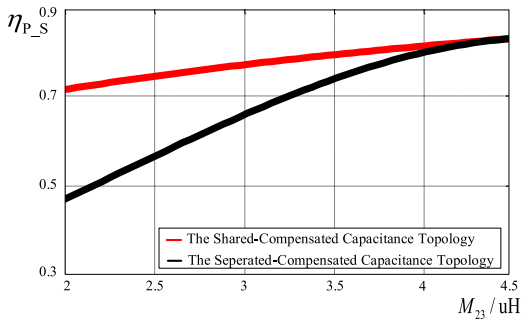

Fig. 10. The comparison of transfer efficiency between different topologies.

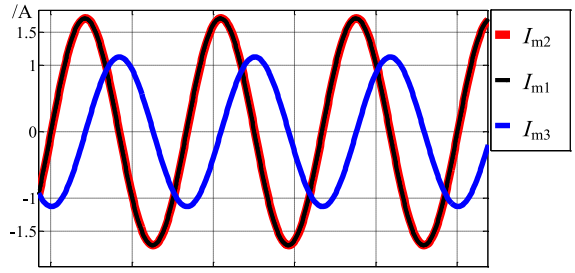

(a)The shared-compensated capacitance topology

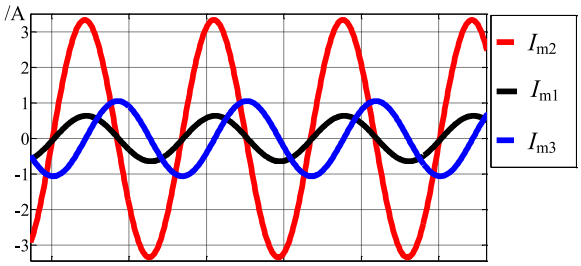

(b)The separated-compensated capacitance topology

Fig. 11. The simulation waveform of I_{m1}, I_{m2} and I_{m3} while M_{13} is 4.5 μH and M_{23} is 2.5 μH.

side to the receiver side is:

$$\eta_{P-S} = \frac{\frac{(\omega M_{13} I_{m1} + \omega M_{23} I_{m2})^2}{R_{L1}}}{\frac{(\omega M_{13} I_{m1} + \omega M_{23} I_{m2})^2}{R_{L1}} + I_{m1}^2 R_1 + I_{m2}^2 R_2} \tag{21}$$

When I_{m1} is equivalent to I_{m2}, equation (21) is simplified to:

$$\eta_{P\_S} = \frac{\omega^2 (M_{13} + M_{23})^2}{\omega^2 (M_{13} + M_{23})^2 + (R_1 + R_2) R_{L1}} \tag{22}$$

The comparison of transfer efficiencies η_{P_S} in shared- or separately-compensated capacitance topologies with different inductances M_{23} is shown in Fig. 10. M_{13} is constant at 4.5 μH. The inductances of the transmitter and receiver coils are all 455 μH, R_1 and R_2 are 3 Ω, R_{L1} is 40 Ω, and the resonance frequency is 600 kHz. From Fig. 10, η_{P_S} is much less sensitive to the change of M_{23} by adopting the shared-compensated capacitance topology. The simulation waveforms of I_{m1}, I_{m2} and I_{m3} obtained from the Simulink software package are given in Fig. 11. It is seen that I_{m1} is still equivalent to I_{m2} for the shared-compensated capacitance topology, while M_{23} is 2.5 μH, and I_{m1} is reduced to only one fifth of I_{m2} for the separately compensated capacitance topology. Therefore, the shared-compensated capacitance topology is more preferable in application.

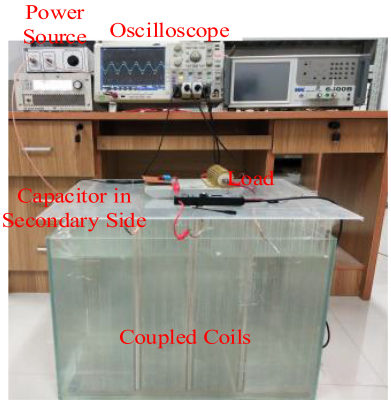

Fig. 12. The physical device of the 1 × 1 × 1 WPT system.

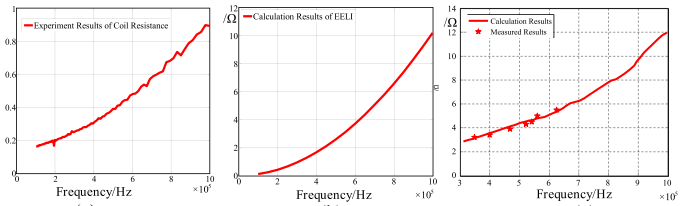

Fig. 13. (a) The measured coil resistance. (b) The EECLI at different frequencies. (c) The total loss resistance Rmea.

V. Experimental Verification

A. Comparison of Transfer Efficiencies in the 1 × 1 and 1 × 1 × 1 Systems

The magnetic cores commonly used in the coil system that helps to increase the mutual inductance are fragile. As the coil should be set at the surface of the underwater vehicles, the magnetic core may be broken in high pressure circumstances. For this reason, coils without magnetic cores are adopted.

Fig. 12 is the physical device of the 1 × 1 × 1 WPT system, and experiments are conducted in saline water with the conductivity of approximately 3.8S/m. The coil resistances R_{Coil} at changing resonance frequencies is given in Fig. 13(a) using the Wayne Kerr impedance analyzer 6500B. The finite element analysis result of EECLI R_{eddy} is shown in Fig. 13(b). By comparing Fig. 13(a) and (b), it is seen that R_{eddy} is much higher than the coil resistance when the resonance frequency is higher than 300 kHz, and the eddy current loss is the major factor decreasing power transfer efficiency in seawater.

The distance between the $Coil_1$ and $Coil_2$ is 120 mm, and the inductance of every coil is approximately 45 μH. The calculated total loss resistance R_{cal} is the sum of R_{Coil} and R_{eddy}. To measure the total loss resistance R_{mea}, $Coil_1$ is put in saline water, and it is serially connected to the load and compensation capacitance. By adjusting the frequency to ensure the receiver circuit is in resonant state, the total resistance R_{total} listed in Table I are measured by the Wayne Kerr impedance analyzer 6500B. While the load resistance R_L is 30 Ω, the measured total

TABLE I
MEASURED PARAMETERS WHILE RL IS 31.5 Ω

C/nF	f/kHz	R_{total}/Ω
3.5	346.8	33.1
2.5	404.7	33.6
2	470	34.1
1.8	523.9	34.5
1.5	543.1	35.2
1.25	562	35.5
1.15	626.2	36

TABLE II
MEASURED PARAMETERS OF 1 × 1 × 1 STRUCTURE

f/kHz	U/V	I/A	I_{m3}/A
346.8	21.4	3.82	1.33
404.7	34.6	3.9	1.73
470	42.3	3.83	1.9
523.9	50.2	3.87	2.11
543.1	55.6	3.81	2.16
562	59.3	3.83	2.21
626.2	75.5	3.87	2.49

TABLE III
MEASURED PARAMETERS OF 1 × 1 STRUCTURE

f/kHz	U/V	I/A	I_{s3}/A
346.8	24.4	3.83	1.35
404.7	35.7	3.87	1.65
470	44.5	3.88	1.8
523.9	50.5	3.73	1.92
543.1	59.9	3.78	2.06
562	63.1	3.82	2.11
626.2	78.8	3.82	2.38

loss resistance R_{mea} is obtained:

$$R_{\text{mea}}=R_{\text{total}}-R_{\text{L}}$$

It is seen in Fig. 13(c) that R_{mea} and R_{cal} are close. Therefore, it can be assumed that the EECLI is serially connected to the circuit. The data of R_{mea} are used to calculate the transfer efficiency in the following experiments. Because the coil parameters are almost the same, the total loss resistance of Coil_2 or Coil_3 is considered to be equal to R_{mea}.

To confirm the improved transfer efficiency of the 1 × 1 × 1 structure and the 1 × 1 structure, the power source voltage U and the current in both transmitter side I, receiver side I_{m3} and I_{s3} are measured. The data are listed in Tables II and III.

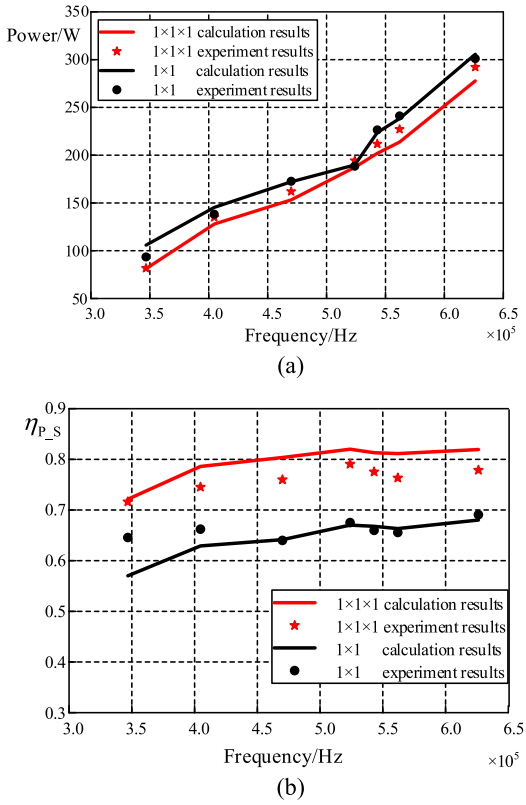

Fig. 14. (a) The calculated and measured powers. (b) The comparison of efficiency from primary side to secondary side.

The total power consumed by the 1 × 1 system is calculated as:

$$P_{cal\_1\times1}=R_{\text{mea}}I^2+R_{\text{mea}}I_{s3}^2+R_{\text{L}}I_{\text{s3}}^2$$
$$=R_{\text{mea}}I^2+R_{\text{total}}I_{\text{s3}}^2$$

The total power consumed by the 1 × 1 × 1 system is calculated as:

$$P_{cal\_1\times1\times1}=R_{\text{mea}}I_{\text{m1}}^2+R_{\text{mea}}I_{\text{m2}}^2+R_{\text{L}}I_{\text{m3}}^2+R_{\text{mea}}I_{\text{m3}}^2$$
$$=\frac{1}{2}R_{\text{mea}}I^2+R_{\text{total}}I_{\text{m3}}^2$$

For both 1×1 and 1 × 1 × 1 structure, the measured power provided by power source in the experiment is:

$$P_{\text{exp}}=UI$$

The calculation transfer efficiency is:

$$\begin{cases}\eta_{\text{P\_S\_cal}}=\frac{I_{\text{s3}}^2(R_3+R_{\text{L}})}{P_{cal\_1\times1}}\\ \text{or}\\ \eta_{\text{P\_S\_cal}}=\frac{I_{\text{m3}}^2(R_3+R_{\text{L}})}{P_{cal\_1\times1\times1}}\end{cases}\tag{23}$$

The experimental transfer efficiency is:

$$\begin{cases}\eta_{\text{P\_S\_exp}}=\frac{I_{\text{s3}}^2(R_3+R_{\text{L}})}{P_{\text{exp\_1\times1}}}\\ \text{or}\\ \eta_{\text{P\_S\_exp}}=\frac{I_{\text{m3}}^2(R_3+R_{\text{L}})}{P_{\text{exp\_1\times1\times1}}}\end{cases}\tag{24}$$

Fig. 14(a) shows the calculated and measured powers. The calculated and measured results are close, which indicates that the circuit model proposed in Section IV can be applied

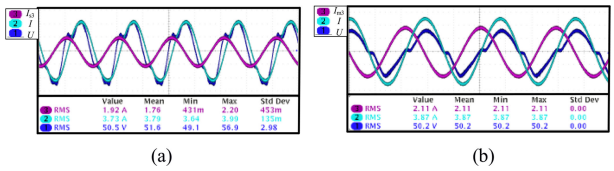

(a) (b)

Fig. 15. (a) The waveform of U, I and I_{s3} for the 1×1 structure. (b) The waveform of U, I and I_{m3} for the $1 \times 1 \times 1$ structure.

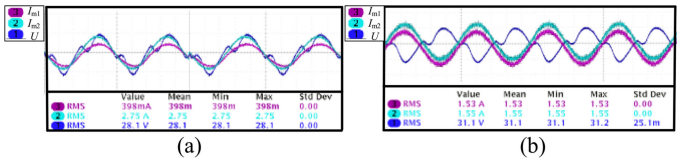

(a) (b)

Fig. 16. (a) The waveform of U, I_{m1}, and I_{m2} for the separately compensated capacitance topology. (b) The waveform of U, I_{m1}, and I_{m2} for the shared-compensated capacitance topology.

in the analysis of the underwater WPT system. Fig. 14(b) shows the transfer efficiency η_{P_S} at different frequencies. The η_{P_S} of the $1 \times 1 \times 1$ system is higher than that of the 1×1 system by approximately 10% at each frequency.

The waveform of U, I and I_{m3} (or I_{s3}) at the highest point of η_{P_S} for the 1×1 and $1 \times 1 \times 1$ structures are shown in Fig. 15. At each resonant frequency, the max current I and I_{m3} in the $1 \times 1 \times 1$ structure are respectively same as those in the 1×1 structure. So, the power transferred to the load for each structure is the same. However, the transfer efficiency of the 1×1 structure is smaller than that of the $1 \times 1 \times 1$ structure according to Fig. 15(b). There are some errors between calculated results and the measured results, but these are attributed to power in the capacitors or conducting wire.

B. The Transfer Efficiencies of Different Circuit Topologies

According to the analysis in Section IV, we found that the shared-compensated capacitance topology is more robust to the change of mutual inductance than that of a separately compensated capacitance topology. To prove this, the following experiments are conducted.

First, the transfer efficiency of the 1×1 system is measured under the conditions that M_{13} is 5.71 μH, the resonant frequency is 523.9 kHz, and R_{L1} is 30 Ω. The measured current in the receiver is 1.92 A, while the transmitter current is 3.73 A, and the power source voltage is 50.5 V. The transfer efficiency η_{P_S} is 67.5%.

Next, the transfer efficiency in the $1 \times 1 \times 1$ system with a separately compensated capacitance topology is measured. M_{13} is still 5.71 μH, but M_{23} is reduced to only 2.5 μH. Other experiment parameters such as resonance frequency and R_{L1} are the same as the first step. The RMS values of I_{m1} and I_{m2} in this topology are 0.398A and 2.75 A, and the receiver side current is 1.28 A. The ratio of I_{m2} to I_{m1} is 6.9. The waveforms of the power source voltage U, I_{m1} and I_{m2} are shown in Fig. 16(a). The measured transfer efficiency η_{P_S} is 63.9%. Additionally, as M_{23} decreases, the transfer efficiency decreases. This implies that in order for the separately compensated capacitance topology to achieve a higher transfer efficiency than the 1×1 structure, the change of M_{23} must be restricted from 2.5 μH to 5 μH.

Finally, for the $1 \times 1 \times 1$ structure with the shared-compensated capacitance topology, η_{P_S} is increased from 73% to 82%, while M_{23} changes from 2.25 μH to 5 μH. When M_{23} is 2.5 μH, the RMS values of I_{m1} and I_{m2} are 1.53A and 1.55 A. The waveforms of the power source voltage U, I_{m1} and I_{m2} are shown in Fig. 16(b), with the ratio of I_{m1} to I_{m2} close to 1. The power source voltage U and the receiver side current I_{m3} are listed in Table IV. The sum of I_{m1} and I_{m2} is 3.86 A. The comparison of the experimental and calculated transfer efficiencies η_{P_S} is given in Fig. 17. The calculation results are obtained through (23), and the experiment results are obtained through (24). According to the experimental results, the shared-compensated capacitance topology is more robust to a change in mutual inductance.

TABLE IV
THE MEASURED PARAMETERS UNDER THE DIFFERENT M_{23} VALUES

M_{23}/MH	U/V	I/A	I_{m3}/A
2.25	37.9	3.86	1.63
2.5	39.8	3.87	1.67
2.9	42.4	3.86	1.76
3.6	36.8	3.88	1.62
3.9	41	3.84	1.85
4.5	45.1	3.81	1.97
5	50.2	3.87	2.11

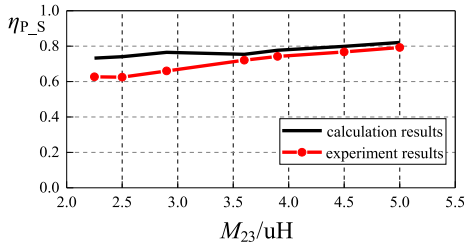

Fig. 17. The transfer efficiency at different M_{23} using shared-compensated topology.

VI. CONCLUSION

A coil structure with two transmitter coils and one receiver coil for reducing eddy current loss in seawater is proposed in this paper. The eddy current loss caused by the transmitter coils in the $1 \times 1 \times 1$ system can be reduced to roughly half of that in the 1×1 system. The experimental results show that the transfer efficiency is improved approximately by 10%. Based on the introduction of equivalent eddy current loss impedance, two kinds of circuit topologies are compared. As the currents in the transmitter coils are mainly determined by the self-inductance of the coils in the shared-compensated capacitance topology, the change of mutual inductance in a certain range has a small influence on the ratio of currents in each transmitter coil. Therefore, the shared-compensated capacitance topology is more robust to the change of mutual inductance. This kind of structure is very useful in underwater vehicle applications.

REFERENCES

[1] L. Chen, S. Liu, Y. C. Zhou, and T. J. Cui, "An optimizable circuit structure for high-efficiency wireless power transfer," *IEEE Trans. Ind. Electron.*, vol. 60, no. 1, pp. 339–349, Jan. 2012.

[2] H. Feng, T. Cai, S. Duan, J. Zhao, X. Zhang, and C. Chen, "An LCC-compensated resonant converter optimized for robust reaction to large coupling variation in dynamic wireless power transfer," *IEEE Trans. Ind Electron.*, vol. 63, no. 10, pp. 6591–6601, Oct. 2016.

[3] Q. Zhu, L. Wang, and C. Liao, "Compensate capacitor optimization for kilowatt-level magnetically resonant wireless charging System," *IEEE Trans. Ind Electron.*, vol. 61, no. 12, pp. 6758–6768, Dec. 2014.
[4] F. Jolani, Y. Yu, and Z. Chen, "A planar magnetically coupled resonant wireless power transfer system using printed spiral coils," *IEEE Antennas Wireless Propag. Lett.*, vol. 13, no. 1, pp. 1648–1651, 2014.
[5] G. Sakemi, T. Yoshimura, and N. Fukuda, "A study of optimization for efficiency and power control in an electromagnetic WPT system," in *Proc. Future Electron Devices, Kansai*, 2013, pp. 108–109.
[6] G. Scarciotti and A. Astolfi, "Moment-based discontinuous phasor transform and its application to the steady-state analysis of inverters and wireless power transfer systems," *IEEE Trans. Power Electron.*, vol. 31, no. 12, pp. 8448–8460, Dec. 2016.
[7] N. S. Gonzalez-Santini, H. Zeng, Y. Yu, and F. Z. Peng, "Z-source resonant converter with power factor correction for wireless power transfer applications," *IEEE Trans. Power Electron.*, vol. 31, no. 11, pp. 7691–7700, Nov. 2016.
[8] C. Y. Liou, C. J. Kuo, and S. G. Mao, "Wireless-power-transfer system using near-field capacitively coupled resonators," *IEEE Trans. Circuits Syst. II, Exp., Briefs*, vol. 63, no. 9, pp. 898–902, Sep. 2016.
[9] F. Lu, H. Zhang, H. Hofmann, and C. C. Mi, "An inductive and capacitive combined wireless power transfer system with LC-compensated topology," *IEEE Trans. Power Electron.*, vol. 31, no. 12, pp. 8471–8482, Dec. 2016.
[10] J. Zhang, X. Yuan, C. Wang, and Y. He, "Comparative analysis of two-coil and three-coil structures for wireless power transfer," *IEEE Trans. Power Electron.*, vol. 32, no. 1, pp. 341–352, Jan. 2017.
[11] S. Li, Z. Liu, H. Zhao, L. Zhu, C. Shuai, and Z. Chen, "Wireless power transfer by electric field resonance and Its application in dynamic charging," *IEEE Trans. Ind. Electron.*, vol. 63, no. 10, pp. 6602–6612, Oct. 2016.
[12] S. Kim, M. Kim, S. Kong, J. J. Kim, and J. Kim, "On-chip magnetic resonant coupling with multi-stacked inductive coils for chip-to-chip wireless power transfer (WPT)," in *Proc. IEEE Int. Symp. Electromagn. Compat.*, 2012, pp. 34–38.
[13] S. Pu and H. T. Hui, "An efficient wireless power transmission system by employing 3×3 stacked coil antenna arrays," in *Proc. IEEE Int. Conf. Rfid Technol. Appl.*, 2016, pp. 171–175.
[14] J. P. K. Sampath, A. Alphones, D. M. Vilathgamuwa, A. Ong, and X. B. Nguyen, "Coil enhancements for high efficiency wireless power transfer applications," in *Proc. Conf. IEEE Ind. Electron. Soc.*, 2014, pp. 2978–2983.
[15] W. Zhang and C. C. Mi, "Compensation topologies of high-power wireless power transfer systems," *IEEE Trans. Veh. Technol*, vol. 65, no. 6, pp. 4768–4778, Jun. 2016.
[16] M. Ogihara, T. Ebihara, K. Mizutani, and N. Wakatsuki, "Wireless power and data transfer system for station-based autonomous underwater vehicles," in *Proc. OCEANS*, 2015, pp. 1–5.
[17] V. Bana, M. Kerber, G. Anderson, J. D. Rockway, and A. Phipps, "Underwater wireless power transfer for maritime applications," in *Proc. Wireless Power Transfer Conf.*, 2015, pp. 1–4.
[18] Z. Cheng, Y. Lei, K. Song, and C. Zhu, "Design and loss analysis of loosely coupled transformer for an underwater high-power inductive power transfer system," *IEEE Trans. Magn.*, vol. 51, no. 7, pp. 1–10, Jul. 2015.
[19] K. Zhang, Y. Duan, Z. Zhu, L. Du, and X. Ren, "A coil structure applied in WPT system for reducing eddy current loss," in *Proc. IEEE Pels Workshop Emerg. Technol.: Wireless Power Transfer*, 2017, pp. 204–206.

Kehan Zhang (M'18) was born in Shaanxi, China, in 1971. He received the B.S. and M.S. degrees from Northwestern Polytechnical University, Xi'an, China, and the Ph.D. degree from the Xi'an Jiaotong University, Xi'an, China.

He is currently an Associate Professor and Master Instructor in Northwestern Polytechnical University. His research interests focus on DSP-based brushless dc motor control system and wireless power transfer.

Xinyi Zhang was born in Henan, China in 1993. She received the B.S. degree from the School of Marine Science and Technology, Northwestern Polytechnical University, Xi'an, China, in 2016. She is currently working toward the M.S. degree in the School of Marine Science and Technology at Northwestern Polytechnical University, Xi'an, China. Her main research interest is wireless power transfer technology.

Zhengbiao Zhu was born in China in 1990. He received the B.S. degree from the School of Marine Science and Technology, Northwestern Polytechnical University, Xi'An, China, in 2015. He is currently working toward the Postgraduate degree in the School of Marine Science and Technology, Northwestern Polytecnical University, Xi'an, China. His current research interests include wireless power transfer and power electronics.

Zhengchao Yan (S'18) received the B.S. degree in mechanical design, manufacturing, and automation, in 2013, from Northwestern Polytechnical University, Xi'an, China, where he is currently working toward the Ph.D. degree. In 2017, he received the funding from China Scholarship Council, and became a joint Ph.D. student in the Department of Electrical and Computer Engineering, San Diego State University, San Diego, CA, USA.

His research interests focus on wireless power transfer, including electromagnetic field calculation, coil design, and compensation topologies.

Baowei Song received the B.S. degree in mechanical engineering from Northwestern Polytechnical University in 1986 and the Ph.D. degree in mechatronic engineering from Northwestern Polytechnical University in 1999. He is currently a Professor and the Vice-President of Northwestern Polytechnical University. His research interests include general technical research of underwater vehicles.

Chunting Chris Mi (S'00–A'01–M'01–SM'03–F'12) received the B.S.E.E. and M.S.E.E. degrees in electrical engineering from Northwestern Polytechnical University, Xi'an, China, in 1985 and 1988, respectively. He received the Ph.D. degree in electrical engineering from the University of Toronto, Toronto, ON, Canada, in 2001.

He is a Professor and Chair of electrical and computer engineering and the Director of the Department of Energy (DOE) -funded Graduate Automotive Technology Education (GATE) Center for Electric Drive Transportation, San Diego State University, San Diego, CA, USA. Prior to joining SDSU, he was with with University of Michigan, Dearborn, from 2001 to 2015. His research interests include electric drives, power electronics, electric machines, renewable-energy systems, and electric and hybrid vehicles.